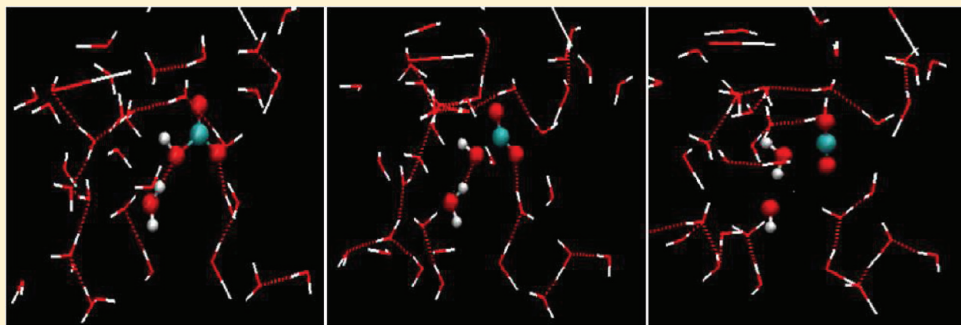


Mechanistic Insights into the Dissociation and Decomposition of Carbonic Acid in Water via the Hydroxide Route: An Ab Initio Metadynamics Study

Mirza Galib* and Gabriel Hanna*

Department of Chemistry, University of Alberta, Alberta, Canada

ABSTRACT:

The dissociation and decomposition of carbonic acid (H_2CO_3) in water are important reactions in the pH regulation in blood, CO_2 transport in biological systems, and the global carbon cycle. H_2CO_3 is known to have three conformers [cis–cis (CC), cis–trans (CT), and trans–trans (TT)], but their individual reaction dynamics in water has not been probed experimentally. In this paper, we have investigated the energetics and mechanisms of the conformational changes, dissociation ($\text{H}_2\text{CO}_3 \rightleftharpoons \text{HCO}_3^- + \text{H}^+$), and decomposition via the hydroxide route ($\text{HCO}_3^- \rightarrow \text{CO}_2 + \text{OH}^-$) of all three conformers of H_2CO_3 in water using Car–Parrinello molecular dynamics (CPMD) in conjunction with metadynamics. It was found that, unlike in the gas phase, the interconversion between the various conformers occurs via two different pathways, one involving a change in one of the two dihedral angles ($\text{O}=\text{C}-\text{O}-\text{H}$) and the other a proton transfer through a hydrogen-bond wire. The free energy barriers/changes for the various conformational changes via the first pathway were calculated and contrasted with the previously calculated values for the gas phase. The CT and TT conformers were found to undergo decomposition in water via a two-step process: first, the dissociation and then the decomposition of HCO_3^- into CO_2 and OH^- . The CC conformer does not directly decompose but first undergoes a conformational change to CT or TT prior to decomposition. This is in contrast with the concerted mechanism proposed for the gas phase, which involves a dehydroxylation of one of the OH groups and a simultaneous deprotonation of the other OH group to yield CO_2 and H_2O . The dissociation in water was seen to involve the repeated formation and breakage of a hydrogen-bond wire with neighboring water molecules, whereas the decomposition is initiated by the diffusion of H^+ away from HCO_3^- ; this decomposition mechanism differs from that proposed for the water route dehydration ($\text{HCO}_3^- + \text{H}_3\text{O}^+ \rightarrow \text{CO}_2 + \text{H}_2\text{O}$), which involves the participation of a nearby H_3O^+ ion. Our calculated pK_a values and decomposition free energy barriers for the CT and TT conformers are consistent with the overall experimental values of 3.45 and 22.28 kcal/mol, respectively, suggesting that the dynamics of the various conformers should be taken into account for a better understanding of aqueous H_2CO_3 chemistry.

I. INTRODUCTION

An understanding of the acid–base chemistry of carbonic acid (H_2CO_3) in water is important in the study of many environmental, biological, and industrial processes.^{1–5} H_2CO_3 is formed when carbon dioxide (CO_2) dissolves in water and reacts reversibly with either water molecules (i.e., water route) or hydroxide ions (i.e., hydroxide route), the latter predominating at higher pHs. The hydration of CO_2 to form H_2CO_3 and the dehydration of H_2CO_3 to form CO_2 are fundamental reactions in the global carbon cycle. For example, the dissolution of atmospheric CO_2 in water to form H_2CO_3 , which then undergoes dissociation to bicarbonate (HCO_3^-) and carbonate (CO_3^{2-})

ions, increases the pH of the oceans.^{6,7} In light of the increasing levels of CO_2 in the atmosphere from anthropogenic sources, many strategies for sequestering it have been proposed, one of which is injection into the ocean.^{1,8} To assess the viability of such an approach, a detailed knowledge of the microscopic mechanisms, energetics, and kinetics of the reactions involving aqueous H_2CO_3 is required. Moreover, the hydroxide route is known to play a fundamental role in the regulation of blood pH and in the

Received: August 12, 2011**Revised:** October 4, 2011**Published:** November 04, 2011

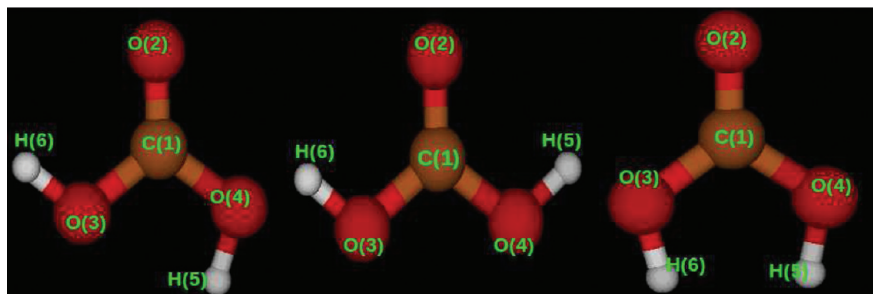


Figure 1. Three conformers of H_2CO_3 . Left: cis–trans (CT) conformer. Center: trans–trans (TT) conformer. Right: cis–cis (CC) conformer.

transport of CO_2 in biological systems.^{9–11} However, this route has yet to be comprehensively investigated theoretically.

H_2CO_3 has been studied in the gas and aqueous phases both theoretically^{12–22} and experimentally.^{2,23–28} Previous theoretical studies have suggested that H_2CO_3 is kinetically stable in the gas phase, having a high activation barrier of ≈ 43 kcal/mol for its decomposition into CO_2 and H_2O ,^{14,26,18} whereas in the presence of water the decomposition is greatly accelerated.²⁶ In the ab initio metadynamics study of gas-phase H_2CO_3 by Kumar et al.,¹⁸ it was found that among the three conformers of H_2CO_3 only the cis–trans (CT) conformer undergoes a direct decomposition into CO_2 and H_2O , whereas the trans–trans (TT) and cis–cis (CC) conformers undergo conformational changes to the CT conformer prior to decomposition. It should be noted that among the three only the CT and TT conformers have been positively identified experimentally via Fourier-transform microwave spectroscopy.^{26,28} Moreover, in ref 17, the energetics of the formation of H_2CO_3 in the aqueous phase via the hydroxide route were calculated using ab initio molecular dynamics. However, the relative stabilities and dissociation/decomposition mechanisms for all three conformers in water have not yet been thoroughly explored.

Previous quantum chemical studies of H_2CO_3 solvated with a few water molecules have shown that there is a systematic reduction in the energy barrier as the number of water molecules is increased from one to three.¹⁵ In the presence of three water molecules, the energy barrier reduced to 20.9 kcal/mol, and the decomposition rate constant increased substantially compared to its gas-phase counterpart but was still a factor of 50 times smaller than the experimentally measured rate constant of 10 s^{-1} at 293 K.¹⁵ Thus, a calculation of the rate constant for a fully solvated system containing many water molecules, rather than just a few, may be necessary to bridge the gap between the theoretical and experimental rate constants. Over the years, the kinetics of the decomposition of H_2CO_3 in water has been investigated by various experimental techniques.^{27,29} More recently, stopped-flow spectrophotometry was used to measure the rate and equilibrium constants of the various reactions involved in the water and hydroxide routes over a wide range of temperatures,²⁷ providing valuable data for comparison in future theoretical studies.

It has been suggested in ref 15 that the decomposition of H_2CO_3 into H_2O and CO_2 is a one-step concerted process. The authors found that the minimum energy path for the dehydration of H_2CO_3 in the presence of water involves the direct participation of one water molecule in a six-membered transition state. However, a recent ab initio molecular dynamics study²¹ has suggested that both the hydration and dehydration of H_2CO_3 are two-step processes, with the dissociation into HCO_3^- and H^+

occurring before the decomposition. The hydration mechanism has been studied directly, but the dehydration mechanism has only been studied in the context of the reverse (hydration) direction. Also, in this study, the hydrogen atoms were replaced by deuterium atoms to use a longer time step. However, the energetics and kinetics of H_2CO_3 are not expected to be the same as for its deuterated counterpart. Furthermore, the reactivity of the various H_2CO_3 conformers in water remains to be explored in detail.

The pK_a of aqueous H_2CO_3 has been a subject of debate for many decades due to the presence of dissolved CO_2 . A pK_a value of 6.35, which corresponds to the equilibrium involving CO_2 , has been commonly reported in chemistry textbooks.^{14,24} However, the true pK_a value, which should not take into account the presence of CO_2 , is substantially lower and was determined to be 3.45 from stopped-flow spectrophotometric measurements²⁹ and also from kinetic fits of ultrafast IR pump–probe data.²⁵ Several theoretical calculations support these experimental results. Using the CBS-QB3 method with CPCM continuum solvation, pK_a values of 3.8, 3.6, and 2.2 were obtained for the TT, CT, and CC conformers, respectively.¹⁶ Using constrained ab initio molecular dynamics, pK_a values of 3.11, 2.60, 3.75, and 0.0 were obtained for the TT, CT_1 (i.e., OH pointing away from carbonyl oxygen), CT_2 (i.e., OH pointing toward carbonyl oxygen), and CC conformers of D_2CO_3 , respectively.²² Recently, a pK_a value of 3.7 was calculated using Car–Parrinello molecular dynamics (CPMD) with metadynamics for the CT_2 conformer.²¹

In this paper, we have carried out CPMD simulations in conjunction with the metadynamics technique for constructing free energy surfaces, to study the mechanisms and energetics of the dissociation and decomposition of the TT, CT, and CC conformers of aqueous H_2CO_3 associated with the hydroxide route. To obtain a more accurate picture of the catalytic role played by water in both the dissociation and decomposition reactions, all of our simulations started with one H_2CO_3 molecule explicitly solvated with 45 water molecules. The energetics of the conformational changes of H_2CO_3 in water were also studied, and the pK_a 's of these conformers were calculated. The remainder of this paper is organized as follows: The computational details are outlined in Section II, the results are presented and discussed in Section III, and the main conclusions are summarized in Section IV.

II. COMPUTATIONAL DETAILS

We have studied the conformational changes of all three conformers of H_2CO_3 (see Figure 1) and their associated dissociation/decomposition reactions in water employing Car–Parrinello molecular dynamics (CPMD)³⁰ in conjunction with

metadynamics.³¹ The hydration of CO₂ yielding H₂CO₃,²¹ autoionization in water,³² and the dissociation of some other acids in water such as formic acid,³³ acetic acid,³⁴ HCl,³⁵ HBr,³⁶ and HF³⁷ have been previously studied using these approaches. CPMD, an ab initio MD technique, solves the time-dependent Schrodinger equation for the ground state electronic wave function (within the Kohn–Sham formulation of density functional theory) to yield the potential energy surface on which the nuclei evolve according to Newton's equations of motion. In contrast to classical MD employing standard nonreactive empirical potentials, this method is capable of treating bond breaking and formation since the potential is calculated on-the-fly.

In general, the dissociation and decomposition of weak acids have relatively high energy barriers compared to $k_B T$ and, as a result, are considered to be rare events. Therefore, one would have to run very long CPMD trajectories to observe these events, which would be computationally very expensive. To circumvent this problem, one may use metadynamics to overcome the high energy barriers in relatively short CPMD simulations and also to calculate free energy profiles. This technique has been reviewed previously,^{38–42} so we only give a brief explanation here. In metadynamics, a history-dependent biasing potential (see eq 1) is added periodically to the natural potential of the system over the course of a trajectory. This biasing potential discourages the system from revisiting points in the configurational space by building up in a given well, to drive the system over to the nearest neighboring well. However, the addition of the history-dependent potential produces an inhomogeneity in the temperature of the system. To remedy this, we have used an extended Lagrangian technique³⁸ in which a fictitious particle is coupled to each collective variable via a harmonic restraining potential. This extended Lagrangian, L_{MTD} , has the following form

$$L_{MTD} = L_{CP} + \frac{\mu}{2} \sum_{\alpha} \dot{s}_{\alpha}^2 - \frac{k}{2} \sum_{\alpha} [S_{\alpha}(r) - s_{\alpha}]^2 - V(t, s) \quad (1)$$

where L_{CP} is the standard CPMD Lagrangian; $S_{\alpha}(r)$ denotes collective variable α ; s_{α} is the coordinate of the fictitious particle that couples to the collective variable (CV) α ; μ is the mass of the fictitious particles; and k is the harmonic spring constant. $V(t, s)$ is the history-dependent biasing potential acting on the fictitious particles, which has the form of a sum of the product of two Gaussians

$$V(t, s) = W \sum_i \exp \left\{ -\frac{(s - s^i)^2}{2(\Delta s')^2} \right\} \times \exp \left\{ -\frac{[(s^{i+1} - s^i) \cdot (s - s^i)]^2}{2(\Delta s'')^4} \right\} \quad (2)$$

where W is the Gaussian height; $s = \{s_1, s_2, \dots\}$ is a vector of the fictitious particle coordinate variables; s^i is a vector of the values of the fictitious particle coordinates at metadynamics step i ; and s' and s'' are Gaussian widths. When all of the potential wells have been filled with these Gaussian hills, the total biasing potential added will give an estimate of the reaction free energy as a function of the fictitious particle coordinates

$$\lim_{t \rightarrow \infty} V(t, s) = -F(s) \quad (3)$$

The pK_a may be calculated from the free energy difference between the products and reactants, ΔF , according to the

thermodynamic relation

$$pK_a = \frac{\Delta F}{k_B T \ln(10)} \quad (4)$$

Our simulations were carried out using version 3.13.2 of the CPMD software⁴³ on a system consisting of a single molecule of H₂CO₃ with 45 water molecules in a cubic cell with periodic boundary conditions and an edge length of 11.3 Å. These parameters give rise to a number density of 0.033 molecules/Å³, which is consistent with the experimental density of water (i.e., 1 g/cm³). The starting configurations for the CPMD runs were taken from the final equilibrated configurations of 100 ps classical MD simulations using the SPC⁴⁴ and Dreiding⁴⁵ force field parameters. Further equilibrations of 10 ps were performed using CPMD, followed by 15 ps CPMD/metadynamics production runs. To generate different initial conditions, we randomized the coordinates and resampled the velocities from a previously equilibrated set of initial conditions, which was followed by further equilibration for 10 ps. These new initial conditions were then used to generate ensembles of trajectories for each conformer and each type of reaction (i.e., conformational changes, dissociation, and decomposition). The valence electrons were treated within the DFT formalism employing the BLYP functional.^{46,47} The BLYP functional has been successfully used recently in the study of the hydrogen bonding (H-bonding) properties²⁰ and the formation of H₂CO₃ in water.²¹ Ultrasoft pseudopotentials^{48,49} were used to describe the interaction of the core electrons with the valence electrons and the nuclei. A plane wave basis set with a cutoff of 40 Ry was employed to expand the Kohn–Sham orbitals. A fictitious electron mass of 600 au and a time step of 4 au (or 0.1 fs) were used. A temperature of 315 K for the ions and a fictitious kinetic energy of 0.06 au for the electronic degrees of freedom were controlled using Nose–Hoover thermostats. Bulk translations and rotations of the system were removed every 100 time steps. It should be noted that using the above parameters, functional, and pseudopotential, we were able to reproduce the various radial distribution functions for all three conformers calculated in ref 20.

For the metadynamics simulations of the conformational changes, the CVs used were the two dihedral angles between the C=O group and the two O–H groups of H₂CO₃. To build up the history-dependent potential, Gaussian hills with heights of 0.56475 kcal/mol for the CC → CT → TT conformational changes (see Figure 2 (upper panel)) and 0.31375 kcal/mol for the TT → CT conformational change (see Figure 2 (lower panel)) were added every 20 MD steps. The kinetic and potential energy parameters corresponding to the fictitious particles which couple to each collective variable were $\mu = 40$ hartee × (au/radians)² and $k = 0.02$ hartee/radians², respectively. The velocities of the fictitious particles were rescaled periodically to maintain their temperature within a range around 315 K. For the metadynamics simulations of the dissociation and decomposition, the CVs used were the C–O and O–H coordination numbers. Coordination numbers are more convenient CVs than bond lengths for describing bond formation/breaking since they are constructed to be 1 when the bond is intact and 0 when the bond is broken. This was accomplished by defining the coordination numbers in the following way

$$C_{ij} = \frac{1 - \left(\frac{d_{ij}}{d_0} \right)^p}{1 - \left(\frac{d_{ij}}{d_0} \right)^{p+q}} \quad (5)$$

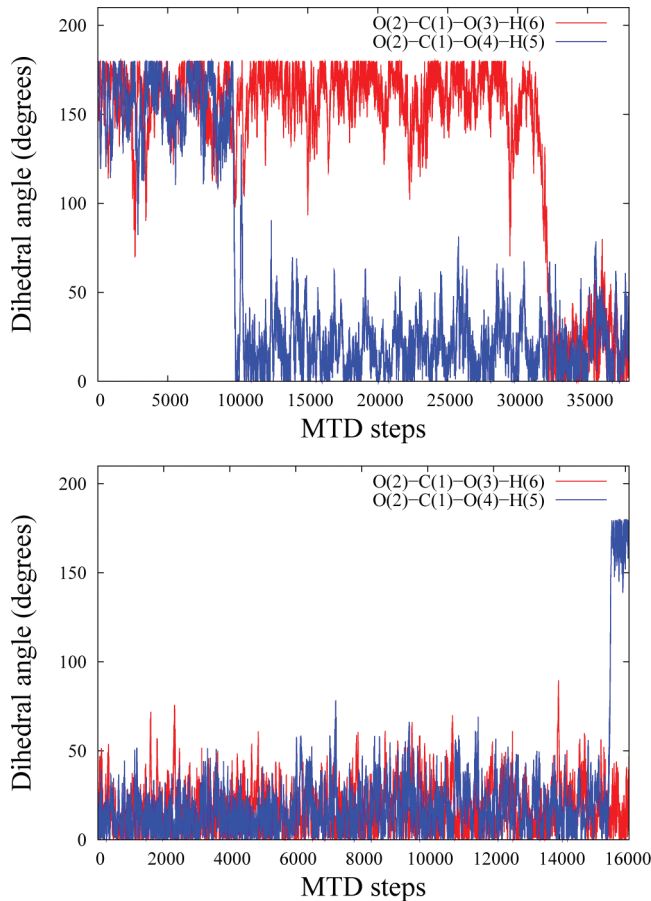


Figure 2. Representative metadynamics trajectories of the two dihedral angles along various conformational changes. Upper panel: CC \rightarrow CT \rightarrow TT. Lower panel: TT \rightarrow CT. Note that each metadynamics (MTD) step = 20 CPMD steps.

where C_{ij} is the coordination number of atom i with respect to atom j ; d_{ij} is the instantaneous distance between atoms i and j ; d_0 is the distance beyond which the bond breaks; and p and q are parameters chosen such that C_{ij} tends to zero beyond d_0 . We have set $p = 6$, $q = 12$, $d_0(\text{C}-\text{O}) = 1.80$, and $d_0(\text{O}-\text{H}) = 1.40$. Gaussian hills with heights of 0.1255 kcal/mol were added every 50 MD steps. The kinetic and potential energy parameters corresponding to the fictitious particles were $\mu = 40 \text{ hartee} \times (\text{au})^2$ and $k = 0.2 \text{ hartee}$, respectively. The velocities of the fictitious particles were rescaled periodically to maintain their temperature within a range around 315 K.

It should be noted that since the history-dependent biasing potential is accumulated iteratively over the course of a metadynamics simulation the system tends to escape from any well via the lowest free energy saddle point. Therefore, metadynamics is useful not only for calculating free energies but also for exploring reaction mechanisms.⁴² However, its reliability strongly depends on the choice of the CVs. If an appropriate set of CVs is employed, metadynamics can give rise to reasonable reaction pathways and shed light on new intermediates.

III. RESULTS AND DISCUSSION

A. Conformational Changes of Carbonic Acid in Water.

As mentioned in Section I, H_2CO_3 has three conformers, namely,

the CT, TT, and CC conformers (see Figure 1), which differ from each other in the relative orientation of the hydroxyl groups.¹⁸ These conformers may be quantitatively distinguished from one another via their two dihedral angles defined by the relative positions of atoms O(2)-C(1)-O(4)-H(5) and O(2)-C(1)-O(3)-H(6) (see Figure 1). In a previous ab initio metadynamics study of gas-phase H_2CO_3 ,¹⁸ it was found that among the three conformers the CC conformer is the least stable (7.9 kcal/mol higher in energy than the CT conformer), and the TT conformer is the most stable (only 1.5 kcal/mol lower in energy than the CT conformer). However, there is some uncertainty as to how their relative stabilities change in the aqueous phase due to the interactions with water molecules.^{16,20} In ref 16, the order of stability was found to be CC < CT < TT using the CBS-QB3 method with CPCM continuum solvation. The free energy barriers for the CT \rightarrow CC and the CT \rightarrow TT conformational changes were determined to be 9.9 and 8.1 kcal/mol, respectively, in the gas phase. However, the free energy changes and barriers in the aqueous phase have not been previously calculated using an explicit solvent. In this study, we have calculated the free energy changes and barriers for the interconversion of all three conformers of H_2CO_3 in water. Initially, we ran several unbiased CPMD trajectories starting from equilibrated configurations of the CC, CT, and TT conformers in water. We observed that the CC conformer remains unchanged in 12 out of 15 trajectories (each 20 ps long) and converts to the CT conformer in the remaining 3, whereas the other two conformers remain unchanged in all 15 trajectories (each 40 ps long). Consequently, unbiased CPMD would be an inefficient way for exploring the reaction dynamics and calculating free energies for these conformational changes due to their relatively high free energy barriers. Thus, we have employed CPMD in conjunction with the metadynamics technique to circumvent this problem. It should be noted that in ref 22 the authors found that the CC conformer is not stable in water, undergoing spontaneous deprotonation in contrast to what we observe. However, our observation is consistent with that reported in ref 16, where the pK_a of the CC conformer was calculated to be 2.2 using the CBS-QB3 method with CPCM continuum solvation. This pK_a value corresponds to a free energy change for the dissociation of the CC conformer of 3.0 kcal/mol. The free energy barrier was not reported, but it must be greater than the free energy change of 3.0 kcal/mol $\approx 5 k_B T$ (at 300 K). Therefore, this reaction is not expected to be accessible by regular CPMD.

In the gas phase, the interconversion between the H_2CO_3 conformers occurs only via a change in one of the two dihedral angles¹⁸ [defined by O(2)-C(1)-O(4)-H(5) and O(2)-C(1)-O(3)-H(6)] since an intramolecular proton transfer is not feasible due to its high energy barrier.¹² Hence, in this metadynamics study, we have used these two dihedral angles as the CVs to investigate the conformational changes in water as the dihedral angles change. Using these two CVs, we ran several metadynamics trajectories starting from different initial conditions for the CC and the TT conformers. The evolution of the CVs as a function of the number of Gaussian hills added throughout a representative metadynamics run starting from the CC and TT conformers is plotted in Figure 2. In the case of the CC conformer [see Figure 2 (upper panel)], we see that after the addition of 9600 Gaussian hills the O(2)-C(1)-O(4)-H(5) dihedral angle changes from 180° to 0°, while the other dihedral angle remains fixed at 180°; i.e., the CC conformer has overcome the barrier and converted to the CT conformer. After the addition of

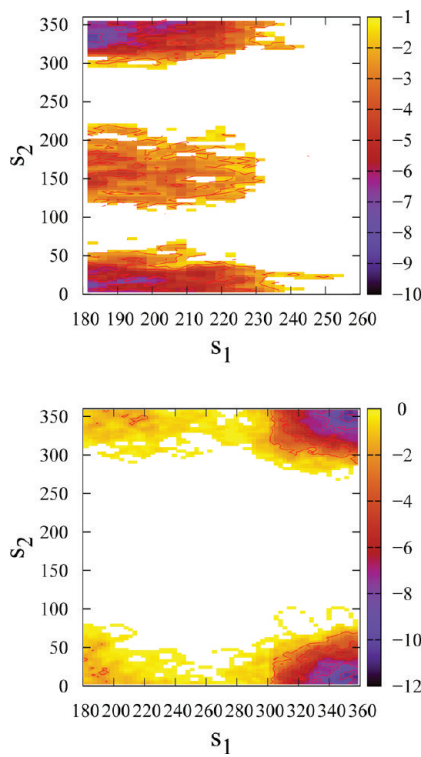


Figure 3. Free energy surfaces (in kcal/mol) as a function of the two auxiliary variables corresponding to the dihedral angles for the various conformational changes of H_2CO_3 . Upper panel: $\text{CC} \rightarrow \text{CT} \rightarrow \text{TT}$. Lower panel: $\text{TT} \rightarrow \text{CT}$. Note that the metadynamics simulations were stopped as soon as the trajectories reached the product wells.

21 253 more Gaussian hills, the $\text{O}(2)-\text{C}(1)-\text{O}(3)-\text{H}(6)$ dihedral angle changes from 180° to 0° , i.e., the CT conformer has overcome the barrier and converted to the TT conformer. In the case of the metadynamics simulation starting from the TT conformer [see Figure 2 (lower panel)], we see that after the addition of 15 537 Gaussian hills the $\text{O}(2)-\text{C}(1)-\text{O}(4)-\text{H}(5)$ dihedral angle changes from 0° to 180° , while the other dihedral angle remains fixed at 0° ; i.e., the TT conformer has overcome the barrier and converted to the CT conformer.

Figure 3 shows the free energy profiles for the conformational changes depicted in Figure 2 as a function of the two auxiliary variables corresponding to the fictitious particles that couple to their respective dihedral angles. The dihedral angles range from -180° to $+180^\circ$ (where the $\pm 180^\circ$ configurations are identical), but the auxiliary variables range from 0° to 360° (where the 0° and 360° configurations are identical). However, due to inversion symmetry, we have reduced the space of one of the dihedral angles to $\{0, 180^\circ\}$, and consequently the space of the corresponding auxiliary variable reduces to $\{180, 360^\circ\}$. The well located near $\{s_1, s_2\} = \{190^\circ, 190^\circ\}$ corresponds to the CC conformer, near $\{s_1, s_2\} = \{190^\circ, 350^\circ\}$ and $\{190^\circ, 20^\circ\}$ correspond to the CT conformer, and near $\{s_1, s_2\} = \{350^\circ, 20^\circ\}$ and $\{350^\circ, 350^\circ\}$ correspond to the TT conformer. The free energy changes and barriers for all of these conformational changes, averaged over our ensemble of five metadynamics runs, are summarized and compared with the corresponding gas-phase values in Table 1. We see that the TT conformer is the most stable conformer in water, as it was found to be in the gas phase. Moreover, it becomes slightly more stable in water than in the gas phase in

Table 1. Energetics for the Conformational Changes of H_2CO_3 in Water^a

conformational change	free energy barrier (kcal/mol)	free energy change (kcal/mol)
$\text{CC} \rightarrow \text{CT}$	3.9 (≈ 2)	—
$\text{CT} \rightarrow \text{CC}$	7.5 (9.9)	3.6 (7.9)
$\text{CT} \rightarrow \text{TT}$	9.0 (8.1)	—
$\text{TT} \rightarrow \text{CT}$	11.5 (9.6)	2.5 (1.5)

^a The values within the brackets are the corresponding gas-phase values from ref 18.

comparison to the CT conformer; i.e., in the gas phase the TT conformer was 1.5 kcal/mol lower in energy than the CT conformer, whereas we found the energy difference between them to be 2.5 kcal/mol (cf. 0.3 kcal/mol in ref 16) in water. Like in the gas phase, the CC conformer is the least stable conformer in water, but it is only 3.6 kcal/mol higher in energy than the CT conformer (cf. 1.9 kcal/mol in ref 16), whereas the energy difference between them was found to be 7.9 kcal/mol in the gas phase. Thus, the use of the CPCM solvation model in ref 16 seems to underestimate the relative energy differences.

B. Dissociation and Decomposition of Carbonic Acid. To understand the chemistry of H_2CO_3 in water, studies of the mechanism, energetics, and kinetics of its dissociation into HCO_3^- (and subsequently CO_3^{2-}) and decomposition into CO_2 are required. Theoretical investigations can give us insight into these aspects by facilitating the interpretation of experimental data and providing a detailed microscopic picture of the underlying reactions. As mentioned in Section I, in the CPMD/metadynamics study by Kumar et al.,¹⁸ it was found that the CC and TT conformers in the gas phase do not undergo decomposition but rather convert to the CT conformer via a change in one dihedral angle before decomposition. They found that the decomposition of the CT conformer occurs via a single-step mechanism. However, in the aqueous phase, the situation is expected to change. For example, Stirling et al.²¹ have already found that the CT conformer undergoes decomposition via a two-step mechanism. Hence, several questions arise:

1. Do the TT and CC conformers undergo decomposition in water?
2. If so, do the reactions involving the CT, TT, and CC conformers take place in a single concerted step or via a stepwise mechanism?
3. How do the energetics of these reactions compare?

In the course of studying the conformational changes, we had observed that unbiased CPMD is inefficient for exploring the reactive dynamics of the various conformers. Therefore, we have also employed the metadynamics technique to study the dissociation and decomposition reactions. As shown in Figure 1, the dissociation and decomposition of H_2CO_3 require the cleavage of two bonds, the $\text{O}(4)-\text{H}(5)$ and $\text{C}(1)-\text{O}(3)\text{H}(6)$ bonds [or, alternatively, the $\text{O}(3)-\text{H}(6)$ and $\text{C}(1)-\text{O}(4)\text{H}(5)$ bonds]. Thus, the use of two bond lengths or, equivalently, two coordination numbers (see Section II) as the CVs is sufficient for exploring the reaction mechanism by metadynamics and for ascertaining whether it is a one-step or multistep process. For the CT conformer, the two O–H bonds are not equivalent and therefore have two different ways to undergo bond cleavage: (i) $\text{C}(1)-\text{O}(3)\text{H}(6)$ and $\text{O}(4)-\text{H}(5)$ and (ii) $\text{C}(1)-\text{O}(4)\text{H}(5)$ and $\text{O}(3)-\text{H}(6)$ [see Figure 1 (left panel)]. Thus, we have used

two sets of CVs, CV set 1 (or CV_1), corresponding to the $\text{C}(1)-\text{O}(3)\text{H}(6)$ and $\text{O}(4)-\text{H}(5)$ coordination numbers, and CV set 2 (or CV_2), corresponding to the $\text{C}(1)-\text{O}(4)\text{H}(5)$ and $\text{O}(3)-\text{H}(6)$ coordination numbers. However, for the TT and the CC conformers, both ways are equivalent (see Figure 1). It should be noted that, using the same CVs, the decomposition of the CT conformer in the gas phase was found to take place via a one-step concerted mechanism in which both bonds break simultaneously to yield CO_2 and H_2O .¹⁸ We ran several independent trajectories using these two CVs starting from the CT, TT, and CC configurations. A set of initial conditions were generated for each by randomizing an equilibrated configuration of the system and rescaling the velocities.

1. Dissociation and Decomposition of the *cis-trans* Conformer. Figure 4 shows snapshots from a representative metadynamics trajectory for the dissociation of a CT H_2CO_3 molecule

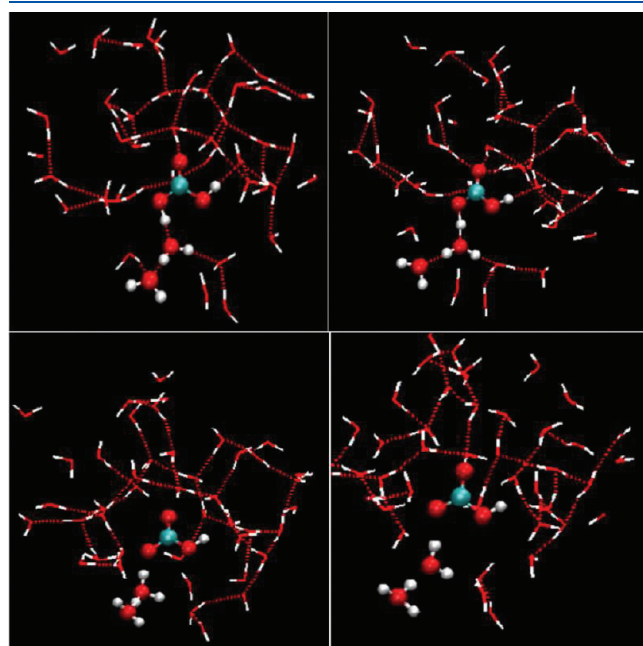


Figure 4. Snapshots of the dissociation of the CT conformer along a representative metadynamics trajectory. Top left: H-bond formation between the donor O in H_2CO_3 and acceptor O in an adjacent water molecule. Top right: Formation of a Zundel-like structure. Bottom left: the O–H bond of H_2CO_3 breaks, leading to the formation of HCO_3^- and H_3O^+ . Bottom right: The excess proton transfers to the next adjacent water molecule, giving rise to a solvent-separated ion pair.

using CV_1 . Initially, the H of the $\text{O}(4)-\text{H}(5)$ hydroxyl group is involved in a H-bond with a water molecule that is H-bonded to other water molecules [see Figure 4 (top left)]. At $t_{\text{MTD}} = 1417$ (where t_{MTD} denotes the number of Gaussian hills added), we see that the H-bonding distance (i.e., the distance between the donor and acceptor O atoms) becomes shorter, forming a Zundel-like structure [see Figure 4 (top right)]. At $t_{\text{MTD}} = 1658$, the O–H bond of H_2CO_3 breaks for the first time due to a solvent fluctuation [see Figure 4 (bottom left)]. Thus, this deprotonation leads to the formation of HCO_3^- and H_3O^+ species. Over the next few hundred metadynamics steps, the proton bounces back and forth between the two species (see Figure 8) until ultimately a proton from the H_3O^+ transfers to an adjacent water molecule via the Grotthuss mechanism. Then, at $t_{\text{MTD}} = 2480$, a solvent-separated state forms with one water molecule between the HCO_3^- and H_3O^+ ions [see Figure 4 (bottom right)]. It should be noted that in some of the metadynamics trajectories generated we also observed that two water molecules separate the ions. At this point, two possible scenarios are observed within our ensemble of trajectories:

1. If the H-bond wire remains unbroken, the proton returns to the HCO_3^- , yielding H_2CO_3 . This is the case for the previously discussed trajectory, where a subsequent protonation occurs (see Figure 5). Deprotonation of H_2CO_3 and reprotonation of HCO_3^- continue to take place as long as the proton wire is intact, giving rise to HCO_3^- and H_3O^+ ions (i.e., the $\text{H}_2\text{CO}_3 \rightleftharpoons \text{HCO}_3^- + \text{H}^+$ equilibrium).
2. If the H-bond wire breaks, the proton diffuses into the bulk via the Grotthuss mechanism as shown in Figure 6. The proton wire formed between the solvent-separated H_3O^+ ion and adjacent water molecules [see Figure 6 (center panel)] breaks, and the excess proton diffuses into the bulk [see Figure 6 (right panel)].

We have also investigated the dissociation of the CT conformer using CV_2 , i.e., the $\text{C}(1)-\text{O}(4)\text{H}(5)$ and $\text{O}(3)-\text{H}(6)$ coordination numbers. The mechanism for the formation of the solvent-separated state (with one or two water molecules between the two ions) is the same as that observed using CV_1 (see Figure 4). At this point, the two scenarios just described for CV_1 are observed. However, in this case a third scenario is also observed. A H-bond wire is formed which connects the proton to the carbonyl oxygen of H_2CO_3 [i.e., O(2)] and thereby leads to the protonation of this oxygen (see Figure 7). In doing so, the CT conformer converts to the TT conformer. This scenario is not observed with CV_1 due to the large distance between the hydroxyl hydrogen, H(5), and the carbonyl oxygen, O(2). For CV_2 , a proton transfer to the carbonyl oxygen takes place due to

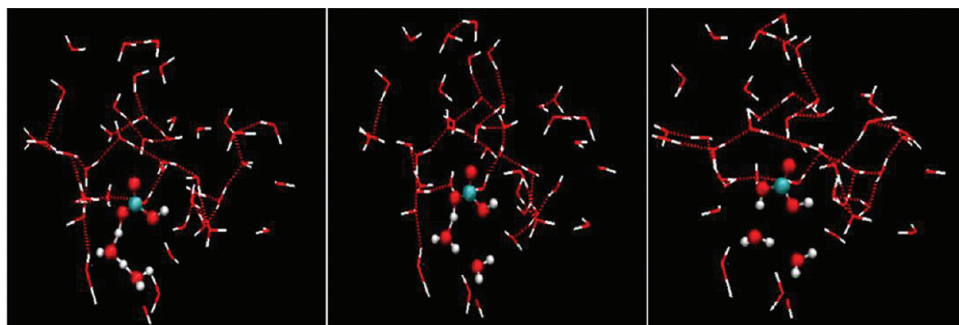


Figure 5. Snapshots along a representative metadynamics trajectory illustrating scenario 1 for the CT conformer (using CV_1). Left: The excess proton returns to the HCO_3^- along a H-bond wire. Center: Zundel-like intermediate forms. Right: Reprotonation of HCO_3^- yields H_2CO_3 .

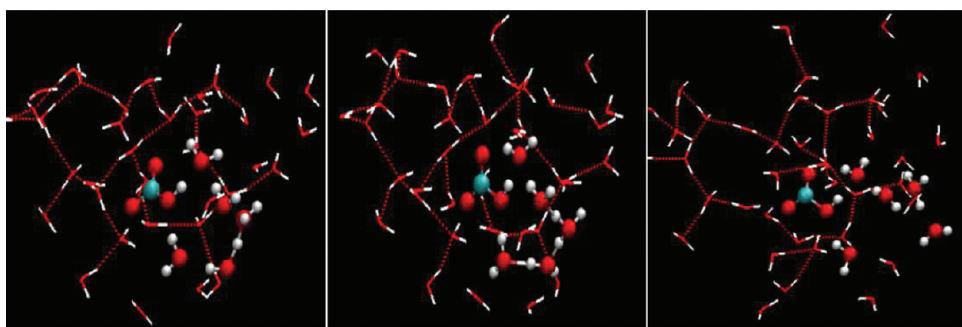


Figure 6. Snapshots along a representative metadynamics trajectory illustrating scenario 2 for the CT conformer (using CV₁). Left: H₃O⁺ and HCO₃⁻ ions are separated by two water molecules. Center: Excess proton resides in H-bond wire. Right: H-bond wire breaks down, and the excess proton diffuses away from the HCO₃⁻.

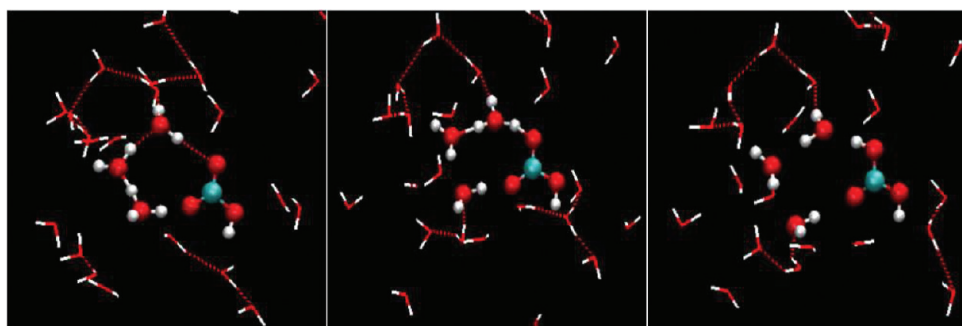


Figure 7. Snapshots along a representative metadynamics trajectory illustrating scenario 3 for the CT conformer (using CV₂). Left: H-bond wire forms. Center: Excess proton transfers along the H-bond wire. Right: Excess proton transfers to O(2) of HCO₃⁻, reforming H₂CO₃.

the fact that H(6) is relatively close to it, facilitating the formation of a H-bond wire connecting the proton through water molecules to O(2). The mechanism observed in this scenario suggests that, unlike in the gas phase, the CT conformer can also undergo a conformational change via an intramolecular proton transfer from O(3) to O(2) along a H-bond wire. The H-bonds between the H₂CO₃ and nearby H₂O molecules facilitate the proton transfer along a H-bond wire, making this route energetically favorable in the aqueous phase.

In summary, we ran a total of 20 trajectories starting from different initial conditions using CV₁ and 15 trajectories using CV₂. For CV₁, 8 metadynamics trajectories underwent dissociation via the mechanism in scenario 1 and 12 trajectories via the mechanism in scenario 2. For CV₂, 2 trajectories underwent dissociation via the mechanism in scenario 1, 9 trajectories via the mechanism in scenario 2, and 4 trajectories via the mechanism in scenario 3.

On the basis of the three scenarios, we see that H-bond wires play a key role in the dissociation of CT H₂CO₃. This is also the case in water autoionization,³² where a H-bond wire between the solvent-separated OH⁻ and H₃O⁺ ions is involved in the dissociation dynamics. However, in a CPMD/transition path sampling study, it was found that the dissociation of acetic acid in water is not driven by the breaking of a H-bond wire between the ions.³⁴ The role of H-bond wires in the dissociation of H₂CO₃ has also been observed in a recent CPMD/metadynamics study.²¹ However, the equilibrium in scenario 1 was observed through two independent simulations, namely, one following the reaction H₂CO₃ → HCO₃⁻ + H₃O⁺ using one set of CVs and the other following the reaction HCO₃⁻ + H₃O⁺ → H₂CO₃ using another

set of CVs. Their trajectory was not evolved for a sufficiently long time to observe both the forward and reverse reactions in a single run, whereas in our simulations both reactions were observed in a single run and using the same sets of CVs. Moreover, scenario 3 was not observed in their simulations due to their choice of CVs. More specifically, starting from HCO₃⁻ and H₃O⁺, only the reprotonation of the hydroxyl oxygen occurs due to the use of an additional CV (i.e., the distance between H₃O⁺ and the hydroxyl oxygen) since their intention was to study the formation of H₂CO₃.

The evolution of the CVs as a function of the number of Gaussian hills added during a representative metadynamics run is plotted in Figure 8. In this figure, the evolution of CV₁ for a trajectory giving rise to scenario 1 is shown. We see that the dissociation begins after the addition of 1417 Gaussian hills, where the magnitude of the fluctuations in the O–H coordination number becomes larger, reflecting the back and forth shuttling of the proton between the donor and acceptor oxygen atoms. After the addition of 2581 hills, the system overcomes the barrier and reaches the product well, giving rise to HCO₃⁻ and H₃O⁺. After the addition of 1785 more hills, the product well becomes filled with hills, and the system then crosses back into the reactant well. This dissociation event involves a change in only one CV (i.e., the O–H coordination number), while the other CV (i.e., the C–O coordination number) remains unchanged.

The dissociation mechanism involves the formation of two intermediates: first, a proton-shared Zundel-like structure (HCO₃^{δ-} · · · H · · · OH₂) forms, which is neither completely covalent nor completely dissociated, followed by the formation of a contact ion pair (HCO₃⁻ · H₃O⁺). The formation of these intermediates was observed by analyzing the following:

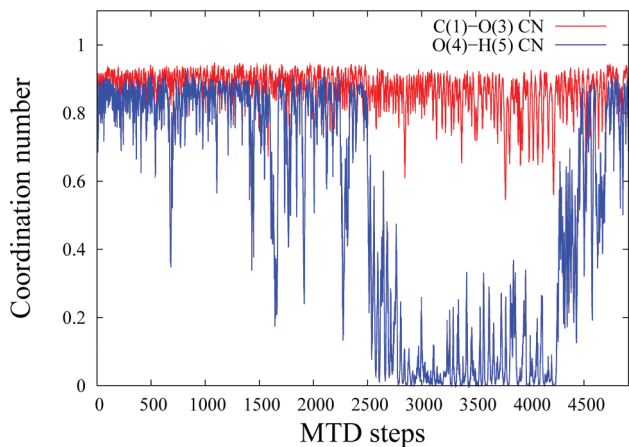


Figure 8. Representative metadynamics trajectories of CV_1 for the CT conformer, illustrating scenario 1. Each MTD step = 50 CPMD steps.

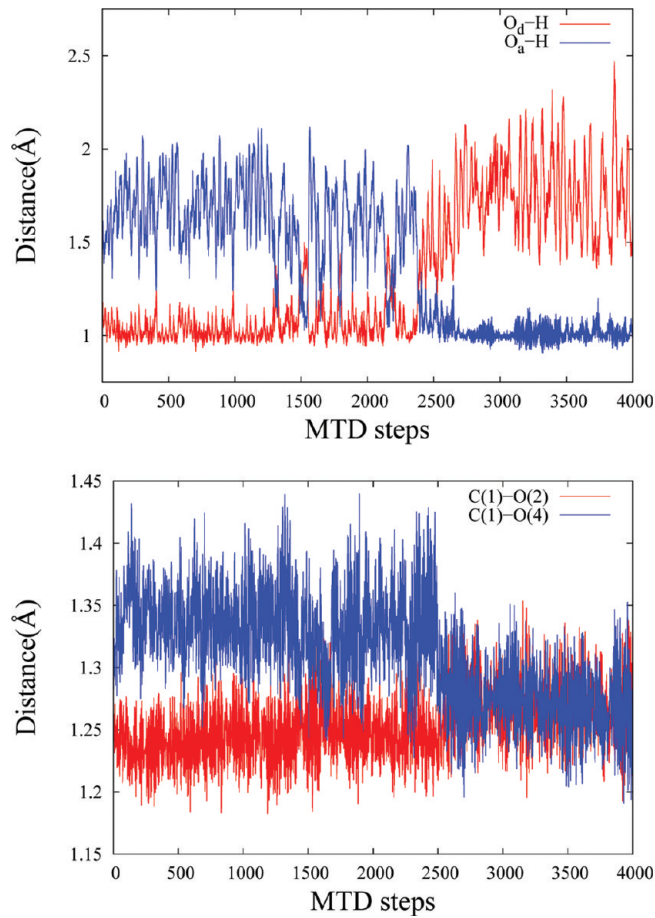


Figure 9. Representative metadynamics trajectories of various interatomic distances for the CT conformer, illustrating scenario 1. Each MTD step = 50 CPMD steps. Upper panel: Trajectories of the (i) O_a -H distance, the distance between the H(6) in H_2CO_3 and the acceptor oxygen in the adjacent water molecule, and the (ii) O_d -H distance, the O(4)-H(6) distance in H_2CO_3 . Lower panel: Trajectories of the C(1)-O(2) and C(1)-O(4) distances.

1. the distance between the proton and the donor O_d (i.e., hydroxyl O in H_2CO_3).

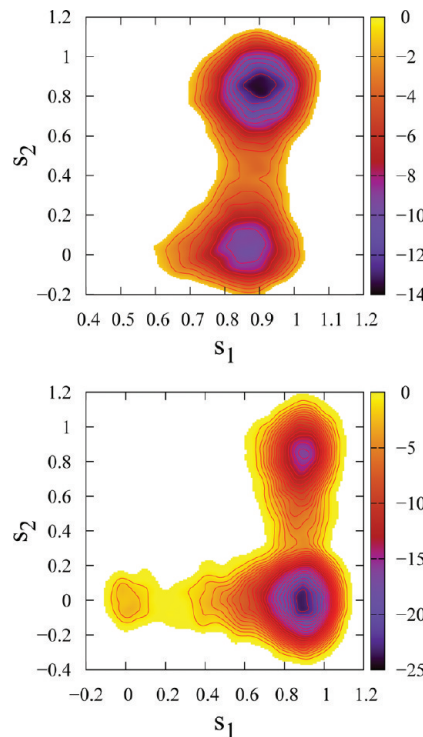


Figure 10. Free energy surfaces (in kcal/mol) as a function of the two auxiliary variables corresponding to the two coordination numbers in CV_1 for the CT conformer. Upper panel: Dissociation observed in scenario 1. Lower panel: Dissociation and decomposition observed in scenario 2.

2. the distance between the proton and the acceptor O_a (i.e., O atom in water molecule).

The upper panel of Figure 9 shows the evolution of these distances along the same representative metadynamics trajectory depicted in Figure 8. The O_a -H distance initially fluctuates around 1.7 Å, which corresponds to the first coordination shell of water molecules around H_2CO_3 as seen in the $\text{H}-\text{O}_\text{a}$ radial distribution function.²⁰ After the addition of 1417 hills, the O_a -H distance decreases and begins to fluctuate around ≈1.5 Å until 2481 hills have been added. During this period, the proton-shared Zundel-like structure exists [see Figure 5 (center panel)]. In this Zundel-like form, HCO_3^- does not give rise to a resonance structure (since the formation of a resonance structure is not energetically favorable),⁵⁰ which is consistent with our observation that the C(1)-O(2) and C(1)-O(4) bond lengths are not equal [see Figure 9 (lower panel)]. After the addition of 2481 hills, the O_d -H and O_a -H distances become equal at ≈1.2 Å, and the contact ion pair forms. At this point, the two C-O bond lengths become equal, and the formation of the resonance structure of HCO_3^- becomes energetically favorable. The contact ion pair is short-lived (separating completely after the addition of 299 more hills) compared to the proton-shared Zundel-like structure. We also investigated the trajectories of these distances for scenario 2 and, like in the case of scenario 1, observed the formation of a Zundel-like intermediate and a contact ion pair.

The free energy profile for the dissociation (i.e., the $\text{H}_2\text{CO}_3 \rightleftharpoons \text{HCO}_3^- + \text{H}^+$ equilibrium observed in scenario 1) as a function of the coordinates of the two fictitious particles coupled to the two coordination numbers in CV_1 is shown in Figure 10

(upper panel). The reactant well is located near $\{s_1 = 0.85, s_2 = 0.85\}$ and the product well near $\{s_1 = 0.85, s_2 = 0\}$. The free energy change between the two wells is 3.8 kcal/mol, and the free energy barrier for the reactant well is 9.7 kcal/mol (and 5.9 kcal/mol for the product well). Our free energy change is close to the previously reported value of 3.51 kcal/mol for D_2CO_3 , calculated using a constrained ab initio MD technique.²² We have also calculated the free energy changes/barriers and the pK_a values for CV_2 . The free energy change is 5.5 kcal/mol, and the free energy barrier for the reactant well is 9.3 kcal/mol (and 3.8 kcal/mol for the product well), which is slightly lower than the previously calculated value for D_2CO_3 .²¹ Our calculated pK_a 's for CT_1 and CT_2 H_2CO_3 are 2.6 and 3.8, respectively, which are very close to the previously calculated values for D_2CO_3 .²² It should be noted that the experimental pK_a for D_2CO_3 was estimated to be ≈ 3.95 ,²⁵ which is considerably higher than those calculated in ref 22. Table 2 summarizes the free energy changes/barriers and

Table 2. Free Energy Barriers/Changes and pK_a Values Corresponding to the Dissociation of the CT Conformer^a

	free energy barrier (kcal/mol)	free energy change (kcal/mol)	pK_a
CT_1	9.7	3.8 (3.51) ²²	2.6 (2.60) ²²
CT_2	9.3 (9.5) ²¹	5.5 (5.06) ²²	3.8 (3.75) ²²

^a The values within the brackets correspond to the results of previous theoretical calculations taken from refs 21 and 22.

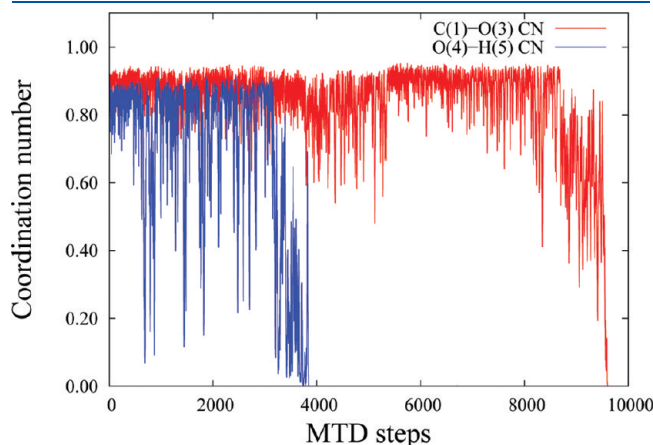


Figure 11. Representative metadynamics trajectories of CV_1 for the CT conformer, illustrating scenario 2. Each MTD step = 50 CPMD steps.

pK_a values for the dissociation and also contains the various previously calculated values.

The lower panel of Figure 10 shows the free energy profile corresponding to scenario 2. In this case, more water molecules separate and solvate the ions, resulting in a product state that is 19 kcal/mol more stable than that in scenario 1. The decomposition of HCO_3^- into CO_2 and OH^- occurs only after the system has undergone scenario 2. This can be seen by examining the representative trajectory presented in Figure 11. After the addition of 8713 hills, the C–O coordination number begins to decrease toward zero, and at zero, the C(1)–O(3) bond breaks, yielding CO_2 and OH^- . This decomposition is the reverse process in the hydroxyl pathway mentioned in Section I. This should be contrasted with the reverse process in the water pathway, where the HCO_3^- undergoes a decomposition into CO_2 and H_2O .²¹ The proposed mechanism for this process first involves a proton transfer from a H_3O^+ to the hydroxyl oxygen of HCO_3^- , to form a coordinated H_2O and thereby weaken the C–O bond, which eventually breaks to yield CO_2 and H_2O . However, we have found that the decomposition via the reverse hydroxyl pathway follows a different mechanism that does not involve the participation of H_3O^+ . Rather, we observe that the C(1)–O(3) bond breaks, yielding OH^- and a bent CO_2 moiety, which straightens to form the linear CO_2 molecule as the OH^- diffuses into the bulk (see Figure 12). The OH^- eventually acquires a proton from an adjacent water molecule, which leads to the diffusion of OH^- via a Grothuss mechanism. The free energy barrier for this decomposition was calculated to be 24.2 kcal/mol (using CV_1) and 26.6 kcal/mol (using CV_2), which are in reasonable agreement with the experimental value of 22.24 kcal/mol, obtained from a spectrophotometric stopped-flow measurement.²⁷

2. Dissociation and Decomposition of the trans-trans Conformer. As stated earlier, the TT conformer also plays an important role in aqueous H_2CO_3 chemistry. Unlike the CT conformer, the two O–H bonds in the TT conformer are symmetrical, and therefore only one set of CVs [i.e., the C(1)–O(3) and O(4)–H(5) coordination numbers] is required. We ran ten metadynamics trajectories using this set of CVs, starting from the TT conformer. It was found that, unlike in the gas phase, the TT conformer in water first undergoes a direct dissociation into HCO_3^- and H^+ , followed by decomposition into CO_2 and OH^- . In the gas phase, the TT conformer does not readily undergo decomposition via the reverse water route since the combination of the H^+ and OH^- ions to form H_2O and break off CO_2 is energetically unfavorable due to the larger distance between these groups.¹⁸ Therefore, the

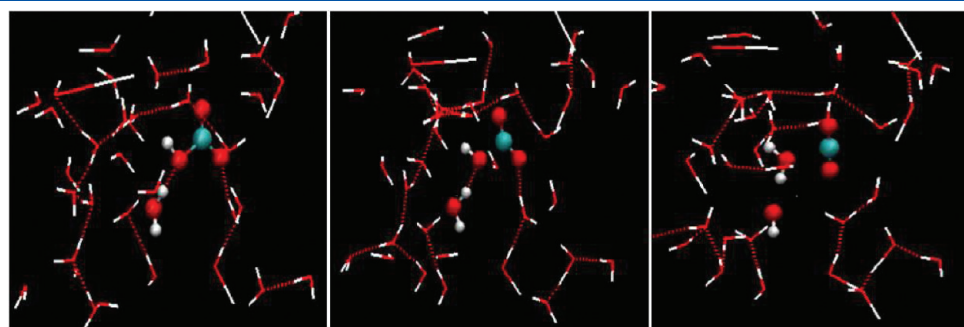


Figure 12. Snapshots of the decomposition of HCO_3^- along a representative metadynamics trajectory. Left: A H-bond forms between O(3) and an adjacent water molecule. Center: C(1)–O(3) bond breaks. Right: CO_2 moiety straightens out to yield the linear CO_2 molecule.

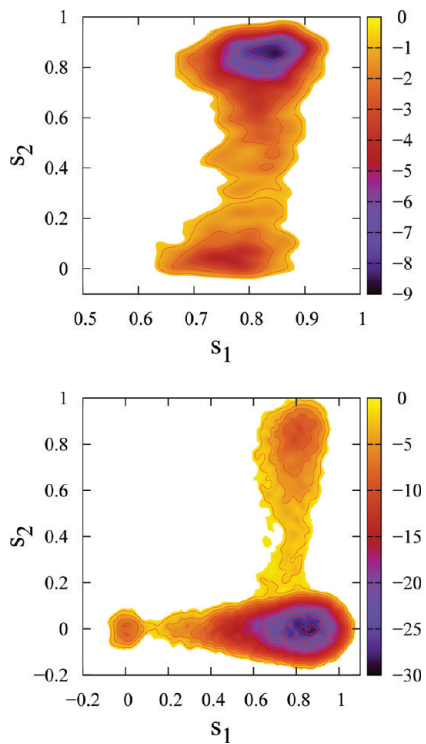


Figure 13. Free energy surfaces (in kcal/mol) as a function of the two auxiliary variables corresponding to the two coordination numbers for the TT conformer. Upper panel: Dissociation observed in scenario 1. Lower panel: Dissociation and decomposition observed in scenario 2.

presence of water allows the TT conformer to undergo decomposition after dissociation, according to the same mechanisms observed in the case of the CT conformer. In addition, after the dissociation takes place, the formation of H-bond wires leads to the same three scenarios we observed in the case of the CT conformer.

The free energy profiles for the dissociation and decomposition reactions were calculated as a function of the coordinates of the two fictitious particles s_1 and s_2 , which couple to the C(1)–O(3) and O(4)–H(5) coordination numbers, respectively. Figure 13 (upper panel) shows the free energy profile for scenario 1, corresponding to the reversible reaction $\text{H}_2\text{CO}_3 \rightleftharpoons \text{HCO}_3^- + \text{H}^+$. The free energy change between the two wells is 4.4 kcal/mol, the pK_a is 3.0, and the free energy barriers for the reactant and product wells are 8.4 and 4.0 kcal/mol, respectively. Our values for the free energy change and pK_a are close to the previously reported values of 4.20 kcal/mol and 3.11, respectively for TT D_2CO_3 , calculated using a constrained ab initio MD technique.²² This pK_a value should be contrasted with the pK_a 's of the CT conformer, which are 2.6 and 3.8 for CT₁ and CT₂, respectively. Thus, we see that the acidity of the TT hydroxyl groups lies in between those of the two different hydroxyl groups in the CT conformer. Figure 13 (lower panel) shows the free energy profile corresponding to scenario 2. In this case, the product state at $\{s_1 = 0.85, s_2 = 0\}$ is 22.23 kcal/mol more stable than that in scenario 1, whereas in the case of the CT conformer, this product state is 18.3 and 22.4 kcal/mol more stable for CV₁ and CV₂, respectively. The free energy barrier for the decomposition was calculated to be 26.2 kcal/mol, which is in reasonable agreement with the overall experimental value of 22.24 kcal/mol.²⁷

3. Dissociation and Decomposition of the cis–cis Conformer. The two O–H groups in the CC conformer are equivalent, like in the case of the TT conformer, and therefore only one set of CVs [i.e., the C(1)–O(3) and O(4)–H(5) coordination numbers] is required. We ran 15 metadynamics trajectories using this set of CVs, starting from the CC conformer. It was found that the CC conformer undergoes dissociation into HCO_3^- and H^+ via the previously observed mechanism, which is then followed by a reprotonation of O(4) or O(2) to yield either the CT or TT conformer. This is similar to what happens in scenario 3 in the cases of the CT and TT conformers. Therefore, like in the gas phase, the CC conformer was found not to directly undergo a decomposition into CO_2 and OH^- but rather to undergo a conformational change to the CT or TT conformer first. However, unlike in the gas phase, the mechanism for the conformational change is an intramolecular proton transfer along a H-bond wire, which is then followed by redissociation and decomposition.

C. Error Estimation. The errors in our metadynamics simulations were estimated using the procedure given in refs 42 and 51. This procedure has also been used in ref 21, where the authors report an error bar of 1.5 kcal/mol. We obtained error bars of 1.3 kcal/mol in the case of the dissociation/decomposition and 1.9 kcal/mol in the case of the conformational changes, based on our ensembles of trajectories. It should be noted that the size of the error bars may be reduced by decreasing the height of the Gaussian hills and the frequency at which they are added, at the cost of increasing the simulation time. Some possible sources of error in these types of simulations have already been discussed in ref 21.

IV. CONCLUSIONS

The mechanisms and energetics of the conformational changes, dissociation, and decomposition of H_2CO_3 in water via the hydroxide route have been investigated using CPMD in conjunction with metadynamics. Like in the gas phase, the TT and CC conformers of H_2CO_3 were found to be the most and least stable in water, respectively. However, the $\text{CC} \rightarrow \text{CT}$ free energy change was found to be 3.9 kcal/mol lower in water than in the gas phase, which indicates that the CC conformer is more stable when solvated by water. Unlike in the gas phase, the interconversion between the various conformers in water was found to occur via two different pathways, one involving a change in one of the two dihedral angles and the other a proton transfer through a H-bond wire. In the gas phase, interconversion between the conformers does not occur via a proton transfer because an intramolecular proton transfer is not energetically feasible. In water, H-bonds between the H_2CO_3 and adjacent H_2O molecules facilitate the proton transfer along a H-bond wire connecting one of the hydroxyl hydrogens to the carbonyl oxygen, making this route energetically favorable. The various energy barriers for the conformational changes involving a change in one of the dihedral angles were calculated. We found that the barrier for $\text{CC} \rightarrow \text{CT}$ is 3.9 kcal/mol, which is about twice that of the gas phase value due to the formation of H-bonds with adjacent water molecules, whereas the barrier for $\text{CT} \rightarrow \text{CC}$ decreases by ≈ 2 kcal/mol relative to that of the gas phase possibly since intermolecular H-bonding with neighboring water molecules reduces the strength of the intramolecular H-bond between H(5) and O(3). In the cases of the $\text{CT} \rightarrow \text{TT}$ and $\text{TT} \rightarrow \text{CT}$ changes, the energy barriers do not change significantly in water compared to the gas phase. This is most likely due to the fact that the dihedral

angle changes are primarily influenced by the intramolecular H-bonds, which are present in both phases.

Unlike in the gas phase, both the CT and TT conformers were found to undergo decomposition via a two-step process: first, dissociation of H_2CO_3 into HCO_3^- and H^+ , followed by the decomposition of HCO_3^- into CO_2 and OH^- . The CC conformer does not undergo a direct decomposition but first converts to either the CT or TT conformer prior to decomposition. The dissociation mechanism for the TT conformer is the same as that for the CT conformer but just has different energetics. More specifically, the dissociation equilibrium involves the formation and subsequent breakage of a H-bond wire with a neighboring water molecule. During this process, two intermediates were observed: (1) a proton-shared Zundel-like structure ($\text{HCO}_3^{\delta-}\cdots\text{H}\cdots\delta^+\text{OH}_2$) and (2) a contact ion pair ($\text{HCO}_3^-\cdot\text{H}_3\text{O}^+$). The decomposition of HCO_3^- involves the breaking of the C–OH bond yielding OH^- and a bent CO_2 moiety, which straightens to form CO_2 as the OH^- diffuses away into the bulk. The OH^- eventually acquires a proton from an adjacent water molecule, which leads to the diffusion of OH^- via the Grotthuss mechanism. Unlike in the case of the water route dehydration, H_3O^+ does not take part in the decomposition via the hydroxide route.

Our metadynamics simulations yielded dissociation free energy barriers of 9.7 and 9.3 kcal/mol for the CT_1 and CT_2 , respectively, and 8.4 kcal/mol for the TT conformer. The calculated free energy changes were 3.8 and 5.5 kcal/mol for CT_1 and CT_2 , respectively, and 4.4 kcal/mol for the TT conformer, which correspond to pK_a values of 2.6, 3.8, and 3.0, respectively. This trend in the pK_a 's is in agreement with a recent constrained ab initio MD calculation²² but different from an ab initio gas-phase calculation¹⁶ with an implicit solvent which found that the TT conformer is less acidic than CT_2 . Therefore, a dynamical treatment with an explicit solvent is required to properly describe the aqueous system. Our values are also supported by the recent experimental measurement of the pK_a of H_2CO_3 , which yielded a value of 3.45,²⁵ and thereby suggest that the presence of all three conformers in water contributes to the overall pK_a . The decomposition free energy barrier was found to be 24.2 and 26.6 kcal/mol for the CT conformer using CV_1 and CV_2 , respectively, and 26.2 kcal/mol for the TT conformer, which are in decent agreement with the experimentally measured value of 22.24 kcal/mol at 298 K²⁷ for the hydroxide route. Our values slightly overestimate the experimental decomposition free energy barrier because the actual temperature in our simulations was most likely lower than 298 K (albeit the simulation temperature was 315 K), as previous CPMD studies have indicated that higher simulation temperatures are required to reproduce the correct behavior at lower temperatures.⁵²

The results presented herein may provide new insights into the understanding of blood pH regulation and CO_2 transport in living systems, for example. The tools and approach used in this paper should be particularly useful in studying the energetics and kinetics of the complete set of reactions carried out by H_2CO_3 and its derivatives in water. In particular, since the previously calculated rate constants for the decomposition of H_2CO_3 via the water route are in major disagreement with experiment, these tools may be used to more accurately calculate this rate constant. Studies of the kinetics of the decomposition of H_2CO_3 via both the water and hydroxide routes are currently underway in our group and will be reported in future publications. This investigation also sets the stage for studies of H_2CO_3 reactivity in diverse

aqueous environments and under different physical conditions, which will have important implications in understanding the role of H_2CO_3 in biological systems and in the development of CO_2 sequestration technologies.

■ AUTHOR INFORMATION

Corresponding Author

*E-mail: mgalib@ualberta.ca; gabriel.hanna@ualberta.ca.

■ ACKNOWLEDGMENT

This project was supported by the National Science and Engineering Research Council of Canada (NSERC), and the computational resources were provided by Compute Canada.

■ REFERENCES

- (1) Haugan, P. M.; Drange, H. *Nature* **1992**, *357*, 318–20.
- (2) Hage, W.; Liedl, K. R.; Hallbrucker, A.; Mayer, E. *Science* **1998**, *279*, 1332–1335.
- (3) Al-Hosney, H. A.; Grassian, V. H. *J. Am. Chem. Soc.* **2004**, *126* (26), 8068–8069.
- (4) Ridgwell, A.; Zeebe, R. E. *Earth Planet. Sci. Lett.* **2005**, *234*, 299–315.
- (5) Hoegh-Guldberg, O.; Mumby, P. J.; Hooten, A. J.; Steneck, R. S.; Greenfield, P.; Gomez, E.; Harvell, C. D.; Sale, P. F.; Edwards, A. J.; Caldeira, K.; Knowlton, N.; Eakin, C. M.; Iglesias-Prieto, R.; Muthiga, N.; Bradbury, R. H.; Dubi, A.; Hatziolos, M. E. *Science* **2007**, *318*, 1737–1742.
- (6) Orr, J. C.; Fabry, V. J.; Aumont, O.; Bopp, L.; Doney, S. C.; Feely, R. A.; Gnanadesikan, A.; Gruber, N.; Ishida, A.; Joos, F.; Key, R. M.; Lindsay, K.; Maier-Reimer, E.; Matear, R.; Monfray, P.; Mouchet, A.; Najjar, R. G.; Plattner, G.-K.; Rodgers, K. B.; Sabine, C. L.; Sarmiento, J. L.; Schlitzer, R.; Slater, R. D.; Totterdell, I. J.; Weirig, M.-F.; Yamanaka, Y.; Yool, A. *Nature* **2005**, *437* (26), 681–686.
- (7) Solomon, S.; Qin, D.; Manning, M.; Chen, Z.; Marquis, M.; Averyt, K.; Tignor, M.; Millers, H. *IPCC*, 2007: Summary for Policymakers. In: *Climate Change 2007: The Physical Science Basis. Contribution of Working Group I to the Fourth Assessment Report of the Intergovernmental Panel on Climate Change*. Technical report, Intergovernmental Panel on Climate Change, 2007.
- (8) Metz, B.; Davidson, O.; Bosch, P.; Dave, R.; Meyer, L. *IPCC*, 2007: Summary for Policymakers. In: *Climate Change 2007: The Physical Science Basis. Contribution of Working Group III to the Fourth Assessment Report of the Intergovernmental Panel on Climate Change*. Technical report, Intergovernmental Panel on Climate Change, 2007.
- (9) Kurtz, I.; Kraut, J.; Ornekian, V.; Nguyen, M. K. *Am. J. Physiol. Renal. Physiol.* **2008**, *294*, F1009–F1031.
- (10) Kikeri, D.; Zeidel, M. L.; Ballermann, B. J.; Brenner, B. M.; Hebert, S. C. *Am. J. Physiol. Cell Physiol.* **1990**, *259*, C471–C483.
- (11) Silverman, D. N.; McKenna, R. *Acc. Chem. Res.* **2007**, *40* (8), 669–675.
- (12) Wight, C. A.; Boldyrev, A. I. *J. Phys. Chem.* **1995**, *99* (32), 12125–12130.
- (13) Nguyen, M. T.; Raspoet, G.; Vanquickenborne, L. G. *J. Phys. Chem. A* **1997**, *101* (40), 7379–7388.
- (14) Loerting, T.; Tautermann, C.; Kroemer, R. T.; Kohl, I.; Hallbrucker, A.; Mayer, E.; Liedl, K. R. *Angew. Chem., Int. Ed. Engl.* **2000**, *39*, 891–894.
- (15) Tautermann, C. S.; Voegele, A. F.; Loerting, T.; Kohl, I.; Hallbrucker, A.; Mayer, E.; Liedl, K. R. *Chem.–Eur. J.* **2002**, *8*, 66–73.
- (16) Tossell, J. A. *Geochim. Cosmochim. Acta* **2005**, *69* (24), 5647–5658.
- (17) Leung, K.; Nielsen, I. M. B.; Kurtz, I. *J. Phys. Chem. B* **2007**, *111*, 4453–4459.
- (18) Kumar, P. P.; Kalinichev, A. G.; Kirkpatrick, R. J. *J. Chem. Phys.* **2007**, *126*, 204315.

- (19) Nguyen, M. T.; Matus, M. H.; Jackson, V. E.; Ngan, V. T.; Rustad, J. R.; Dixon, D. A. *J. Phys. Chem. A* **2008**, *112*, 10386–10398.
- (20) Kumar, P. P.; Kalinichev, A. G.; Kirkpatrick, R. J. *J. Phys. Chem. B* **2009**, *113*, 794–802.
- (21) Stirling, A.; Papai, I. *J. Phys. Chem. B* **2010**, *114* (50), 16854–16859.
- (22) Liu, X.; Lu, X.; Wang, R.; Zhou, H. *J. Phys. Chem. A* **2010**, *114* (49), 12914–12917.
- (23) Terlouw, J. K.; Lebrilla, C. B.; Schwarz, H. *Angew. Chem., Int. Ed. Engl.* **1987**, *26*, 354–355.
- (24) Ludwig, R.; Kornath, A. *Angew. Chem., Int. Ed. Engl.* **2000**, *39*, 1421–1423.
- (25) Adamczyk, K.; Prmont-Schwarz, M.; Pines, D.; Pines, E.; Nibbering, E. T. *J. Science* **2009**, *326*, 1690–1694.
- (26) Mori, T.; Suma, K.; Sumiyoshi, Y.; Endo, Y. *J. Chem. Phys.* **2009**, *130*, 204308.
- (27) Wang, X.; Conway, W.; Burns, R.; McCann, N.; Maeder, M. *J. Phys. Chem. A* **2010**, *114*, 1734–1740.
- (28) Mori, T.; Suma, K.; Sumiyoshi, Y.; Endo, Y. *J. Chem. Phys.* **2011**, *134*, 044319.
- (29) Soli, A. L.; Byrne, R. H. *Mar. Chem.* **2002**, *78* (2–3), 65–73.
- (30) Car, R.; Parrinello, M. *Phys. Rev. Lett.* **1985**, *55*, 2471–2474.
- (31) Laio, A.; Parrinello, M. *Proc. Natl. Acad. Sci. U.S.A.* **2002**, *99*, 12562.
- (32) Geissler, P. L.; Dellago, C.; Chandler, D.; Hutter, J.; Parrinello, M. *Science* **2001**, *291*, 2121–2124.
- (33) Lee, J.-G.; Asciutto, E.; Babin, V.; Sagui, C.; Darden, T.; Roland, C. *J. Phys. Chem. B* **2006**, *110*, 2325–2331.
- (34) Park, J. M.; Laio, A.; Iannuzzi, M.; Parrinello, M. *J. Am. Chem. Soc.* **2006**, *128*, 11318–11319.
- (35) Laasonen, K. E.; Klein, M. L. *J. Phys. Chem. A* **1997**, *101* (01), 98–102.
- (36) Raugei, S.; Klein, M. L. *J. Am. Chem. Soc.* **2001**, *123* (38), 9484–9485.
- (37) Kim, D.; Klein, M. L. *J. Am. Chem. Soc.* **1999**, *121* (48), 11251–11252.
- (38) Iannuzzi, M.; Laio, A.; Parrinello, M. *Phys. Rev. Lett.* **2003**, *90* (23), 238302.
- (39) Micheletti, C.; Laio, A.; Parrinello, M. *Phys. Rev. Lett.* **2004**, *92*, 170601.
- (40) Martok, R.; Laio, A.; Bernasconi, M.; Ceriani, C.; Raiteri, P.; Zipoli, F.; Parrinello, M. *Comput. Crystallogr.* **2005**, *220*, 489–498.
- (41) Ensing, B.; Laio, A.; Parrinello, M.; Klein, M. L. *J. Phys. Chem. B* **2005**, *109* (4), 6676–6687.
- (42) Laio, A.; Gervasio, F. L. *Rep. Prog. Phys.* **2008**, *71*, 126601–126622.
- (43) Copyright IBM Corp 1990–2008, Copyright MPI für Festkörperforschung Stuttgart 1997–2001. CPMD V3.13.2.
- (44) Berendsen, H.; Postma, J.; van Gunsteren, W.; Hermans, J. In *Intermolecular Forces*; Pullman, B., Ed.; Reidel: Dordrecht, 1981; Chapter Interaction models for water in relation to protein hydration, pp 331–342.
- (45) Mayo, S. L.; Olafson, B. D.; Goddard, W. A. *J. Phys. Chem.* **1990**, *94* (26), 8897–8909.
- (46) Becke, A. D. *Phys. Rev. A* **1988**, *38* (6), 3098–3100.
- (47) Lee, C.; Yang, W.; Parr, R. G. *Phys. Rev. B* **1988**, *37* (2), 785–789.
- (48) Vanderbilt, D. *Phys. Rev. B* **1990**, *41* (11), 7892–7895.
- (49) Laasonen, K.; Pasquarello, A.; Car, R.; Lee, C.; Vanderbilt, D. *Phys. Rev. B* **1993**, *47* (16), 10142–10153.
- (50) Thomas, V.; Maurer, P.; Iftimie, R. *J. Phys. Chem. B* **2010**, *114*, 8147–8155.
- (51) Bussi, G.; Laio, A.; Parrinello, M. *Phys. Rev. Lett.* **2006**, *96*, 090601.
- (52) Schwegler, E.; Grossman, J. C.; Gygi, F.; Galli, G. *J. Chem. Phys.* **2004**, *121* (11), 5400–5409.